Novel High Step-Up DC–DC Converter for Fuel Cell Energy Conversion System

Shih-Kuen Changchien, Tsorng-Juu Liang, *Member, IEEE*, Jiann-Fuh Chen, *Member, IEEE*, and Lung-Sheng Yang

***Abstract*—A novel high step-up dc–dc converter for fuel cell energy conversion is presented in this paper. The proposed converter utilizes a multiwinding coupled inductor and a voltage doubler to achieve high step-up voltage gain. The voltage on the active switch is clamped, and the energy stored in the leakage inductor is recycled. Therefore, the voltage stress on the active switch is reduced, and the conversion efficiency is improved. Finally, a 750-W laboratory prototype converter supplied by a proton exchange membrane fuel cell power source and an output voltage of 400 V is implemented. The experimental results verify the performances, including high voltage gain, high conversion efficiency, and the effective suppression of the voltage stress on power devices. The proposed high step-up converter can feasibly be used for low-input-voltage fuel cell power conversion applications.**

***Index Terms*—Coupled inductor, fuel cell, high step-up dc–dc converter, leakage inductor, voltage doubler.**

I. Introduction

The DEVELOPMENT of "green power" generation has recently become very important to address environmental pollution and the problem of exhaustion of fossil energy reserves. Fuel cells represent one of the most efficient and effective alternative renewable energy sources for many applications, such as hybrid electric vehicles, uninterruptible power supplies, telecom back-up facilities, and portable electronics [1]–[4].

Fuel cells generate electricity via chemical reactions between hydrogen and oxygen. Much research on fuel cells and fuel cell stacks can be found in the literature [5], [6]. The proton exchange membrane fuel cell (PEMFC) is one of the most commonly used fuel cell for low-to-middle power generation systems. The PEMFC transfers hydrogen and oxygen energy into electrical energy and produces water and heat in the surface of catalytic particles. The reactions on the anode and the cathode and the global reaction of the PEMFC can be described as anode reaction

$$\mathrm{H_2} \rightarrow 2\mathrm{H^+} + 2e^- \tag{1}$$

cathode reaction

$$\frac{1}{2}\mathrm{O_2} + 2\mathrm{H^+} + 2e^- \rightarrow \mathrm{H_2O} \tag{2}$$

and global reaction

$$\mathrm{H_2} + \frac{1}{2}\mathrm{O_2} \rightarrow \mathrm{H_2O} + \mathrm{heat} + \mathrm{electricity}. \tag{3}$$

Fig. 1 shows a general fuel-cell power generation system. Generally, the output voltage of the fuel cell stacks V_{FC} is varied from 24 to 40 V depending on the output power. In order to obtain a utility ac source (220-V rms at 50/60 Hz) from a fuel cell, a high dc bus voltage (380–400 V) is required at the input of the dc–ac inverter. Therefore, a high step-up dc–dc converter is needed to boost the low voltage at the fuel cell stacks into the high voltage at the dc bus.

In general, a conventional boost converter can be adopted to provide a high step-up voltage gain with a large duty ratio. However, the conversion efficiency and the step-up voltage gain are limited due to the constraints of the losses of power switches and diodes, the equivalent series resistance of inductors and capacitors, and the reverse-recovery problem of diodes [7], [8]. Therefore, a step-up converter with a reasonable duty ratio to achieve high efficiency and high voltage gain is very important for a fuel-cell power generation system.

Isolated converters, such as forward, flyback, half-bridge, full-bridge, and push–pull types, can be used to convert a low voltage into a higher output voltage by adjusting the turn ratio of the transformer. However, the active switch of these converters will suffer very high voltage stress and high power dissipation due to the leakage inductance of the transformer [9], [10]. To reduce the voltage spike, a resistor–capacitor–diode snubber can be employed to limit the voltage stress on the active switch. However, the efficiency will be reduced [11]. Nondissipative snubbers and active clamp techniques have been adopted to recycle the energy stored in the leakage inductor and to suppress the voltage spike across the active switch [12]–[15]. However, the cost will be increased due to the additional power switch, and high side driver is required.

In order to improve the conversion efficiency and to increase the step-up voltage gain without using the isolation transformer, many step-up converters based on a boost converter with a coupled inductor have been proposed [16]–[28]. High step-up converters with a low input current ripple based on the coupled inductor have been developed [16], [17]. The low input current ripple of these converters is realized by using an additional LC circuit with a coupled inductor. However, leakage inductance issues that relate to the voltage spike and the efficiency remain

Manuscript received February 27, 2009; revised May 18, 2009; accepted June 8, 2009. Date of publication October 23, 2009; date of current version May 12, 2010. This work was supported in part by the Bureau of Energy, Ministry of Economic Affairs, under Grant 98-D0204-2 and in part by the National Science Council of Taiwan under Project NSC 98-2221-E-006-247-MY3.

S.-K. Changchien is with the Department of Electrical Engineering, National Cheng Kung University, Tainan 701, Taiwan, and also with the Department of Electrical Engineering, Chienkuo Technology University, Changhua City, Taiwan (e-mail: ccsk@ctu.edu.tw).

T.-J. Liang, J.-F. Chen, and L.-S. Yang are with the Department of Electrical Engineering, National Cheng Kung University, Tainan 701, Taiwan (e-mail: tjliang@mail.ncku.edu.tw; chenjf@mail.ncku.edu.tw; yanglungsheng@yahoo.com.tw).

Digital Object Identifier 10.1109/TIE.2009.2026364

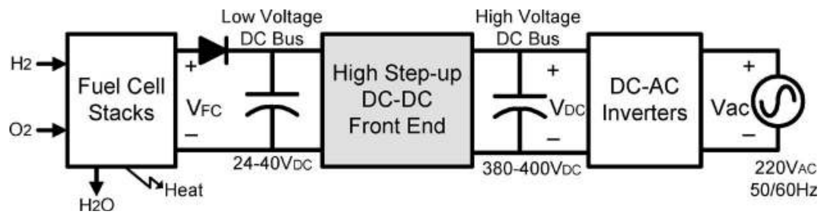

Fig. 1. General fuel-cell power generation system with a high step-up converter.

significant. An integrated boost–flyback converter based on a coupled inductor with high efficiency and high step-up voltage gain has been presented [18], [19]. The energy stored in the leakage inductor is recycled into the output during the switch-off period. Thus, the efficiency can be increased, and the voltage stress on the active switch can be suppressed. Many step-up converters, which use an output voltage stacking to increase the voltage gain, are presented [20]–[23], [31]. A high step-up dc–dc converter with an integrated coupled inductor and a common mode electromagnetic interference reduction filter is presented [20]. A Sepic–flyback converter with a coupled inductor and an output voltage stacking is developed [21]. A high step-up converter, which utilizes a coupled inductor and a voltage doubler technique on the output voltage stacking to achieve a high step-up voltage gain, is introduced [22]. A high step-up boost converter that uses multiple coupled inductors for the output voltage stacking is proposed [23]. High voltage gain can also be obtained with a tapped secondary winding of the transformer and input–output voltage cascoded for the extended forward-type converters of the high step-up converters [31]. However, extra devices, such as diodes and output capacitors, are needed for these converters. Additionally, step-up converters, which use a voltage lift, are introduced [24], [25]. Since the switch must suffer high current during the switch-on period, this technique is appropriate for low-output-power applications. High step-up converters with low voltage stress on the active switch can be realized by using the integrated coupled inductor and the voltage-lift technique [26]–[28]. Since the low voltage rating and the low conducting resistance $r_{ds(\mathrm{on})}$ of the power switch are used for these converters, the high conversion efficiency can be achieved. However, the requirement for a coupled inductor with a high coupling coefficient will result in manufacturing difficulty and cost increment. A high step-up converter, which uses a three-state switching cell and a voltage multiplier stage based on capacitors, can achieve high step-up gain [29], [30]. The voltage gain can be raised by adding the voltage multiplier stages of the capacitors. Since the two switches operate as interleaved operation, the size of the inductor can be reduced because the operating frequency of the inductor is double of the switching frequency. Moreover, the conduction losses can be reduced due to the current share of the active switches. Thus, this converter is suitably used for high-power applications. However, two switches are needed for the interleaved operation of this high-voltage-gain boost converter.

This paper presents a novel high-efficiency high step-up dc–dc converter, which has only one active switch. The proposed converter uses a three-winding coupled inductor and a voltage doubler on the output to achieve a high dc voltage. The proposed converter has the following features:

1) high step-up voltage gain;
2) energy stored in the leakage inductor is recycled to increase efficiency;
3) voltage stress on the active switch is clamped; thus, a power switch with a low voltage rating and a low on resistance $r_{ds(\mathrm{on})}$ can be adopted.

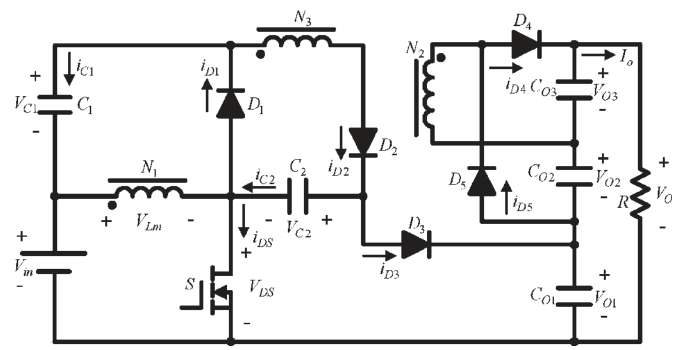

Fig. 2. Circuit configuration of the proposed converter.

II. Operation Principle of the Proposed Converter

Fig. 2 shows the circuit configuration of the proposed converter. This converter consists of a dc input voltage V_{in}, one power switch, one three-winding coupled inductor, five diodes, and five capacitors. The dc input voltage V_{in} and the circuit components N_1, S, D_1, and C_1 are operated as a boost converter with an input voltage cascode. The energy stored in the leakage inductor can be recycled. Thus, the efficiency can be improved. Also, the voltage across switch S is clamped effectively. The voltage doubler is composed of N_2, D_4, D_5, C_{O2}, and C_{O3}, which is stacked on the output to increase the voltage gain. The three-winding coupled inductor is used to provide high step-up voltage gain by adjusting the turn ratios of the windings.

To simplify the circuit analysis, the following conditions are assumed.

1) Capacitors C_1, C_2, C_{O1}, C_{O2}, and C_{O3} are large enough. Thus, V_{C1}, V_{C2}, V_{O1}, V_{O2}, and V_{O3} are considered as constant in one switching period.
2) The power MOSFET and the diodes are treated as ideal, but the parasitic capacitance of the power switch is considered.
3) The turn ratios of the coupled inductor are $n_2 = N_2/N_1$ and $n_3 = N_3/N_1$.

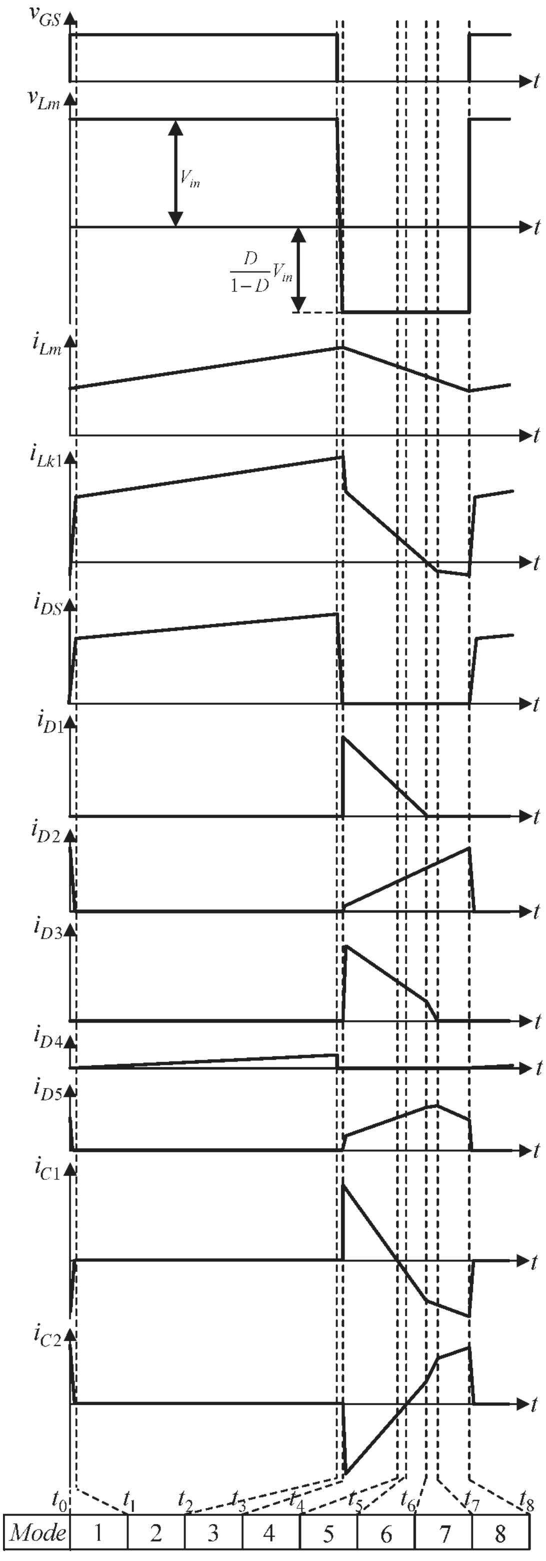

Fig. 3. Some typical waveforms under CCM operation in one switching period.

A. Continuous Conduction Mode (CCM)

Based on the aforementioned assumption, there are eight operating modes in one switching period of the proposed converter under CCM. Fig. 3 illustrates some typical key waveforms under CCM operation in one switching period. The operating modes are described as follows.

Mode 1 (t_0-t_1)*:* At $t = t_0$, S is turned on, D_2 and D_5 are turned on, and D_1, D_3, and D_4 are turned off. Fig. 4(a) shows the current-flow path of the proposed converter in this mode. In this interval, the energy of C_S is discharged rapidly. The energy stored in L_{k3} is released to C_2, and the energy stored in L_{k2} is released to C_{O2}. Thus, i_{D2}, i_{D5}, and i_{C2} are decreased. At $t = t_1$, i_{D2} is equal to zero; this mode is ended.

Mode 2 (t_1-t_2)*:* In this mode, S is kept switched on, D_1, D_2, D_3, and D_5 are turned off, and D_4 is turned on. Fig. 4(b) depicts the current-flow path of this mode. In this interval, the inductors L_{k1} and L_m are charged from the dc input voltage V_{in}, and the energy is transferred to C_{O3} and the load. The currents i_{Lk1} and i_{Lm} are increased. The voltage across C_{O3} is approximately charged to $n_2 V_{\text{in}}$. The load energy is supplied by the output capacitors C_{O1}, C_{O2}, and C_{O3}. This mode is ended at $t = t_2$ when S is turned off.

Mode 3 (t_2-t_3)*:* At $t = t_2$, S is turned off, and D_1, D_2, D_3, D_4, and D_5 are also turned off. Fig. 4(c) illustrates the current-flow path of the proposed converter in this mode. In this interval, the energy of the dc source is released to L_{k1}, L_m, and C_S. Therefore, the voltage across S is increased linearly until $t = t_3$; meanwhile, $V_{DS} = V_{\text{in}} + V_{C1}$. V_{O3} is maintained at about $n_2 V_{\text{in}}$. The load energy is supplied by the output capacitors C_{O1}, C_{O2}, and C_{O3}.

Mode 4 (t_3-t_4)*:* At $t = t_3$, $V_{DS} = V_{\text{in}} + V_{C1}$. In this interval, S is still off, D_1, D_2, D_3, and D_5 are turned on, and D_4 is turned off. Fig. 4(d) shows the current-flow path of the proposed converter in this mode. The energies stored in L_{k1} and L_m are released to capacitor C_1. i_{D1} is decreased linearly. Moreover, the energy stored in L_m is released to C_{O2} via N_2. The energies stored in L_m and C_2 are also released to C_{O1}. Thus, i_{D2} and i_{D5} are increased linearly. The leakage inductor energy can thus be recycled, and the voltage stress of the switch can be limited. This mode is ended at $t = t_4$ when $i_{C1} = 0$.

Mode 5 (t_4-t_5)*:* At $t = t_4$, S is kept switched off, D_1, D_2, D_3, and D_5 are turned on, and D_4 is turned off. Fig. 4(e) illustrates the current-flow path of the proposed converter in this mode. In this interval, the energies stored in C_1, C_2, L_{k1}, and L_m are released to capacitor C_{O1}. The energy stored in L_m is released to C_{O2} via N_2. This mode is ended at $t = t_5$ when $i_{C2} = 0$.

Mode 6 (t_5-t_6)*:* At $t = t_5$, S is kept switched off, D_1, D_2, D_3, and D_5 are turned on, and D_4 is turned off. Fig. 4(f) shows the current-flow path of the proposed converter in this mode. In this interval, the energies stored in C_1, L_{k1}, and L_m are kept released to capacitor C_{O1}. The energy stored in L_m is kept released to C_2 and C_{O2}. This mode is ended at $t = t_6$ when $i_{D1} = 0$ and $i_{Lk1} = 0$.

Mode 7 (t_6-t_7)*:* At $t = t_6$, S is turned off, D_2, D_3, and D_5 are turned on, and D_1 and D_4 are turned off. Fig. 4(g) shows the current-flow path of the proposed converter in this mode. In this interval, the energy stored in L_m is released to C_2, C_{O1}, and C_{O2} via N_2 and N_3. This mode is ended at $t = t_7$ when $i_{D3} = 0$.

Mode 8 (t_7-t_8)*:* At $t = t_7$, $i_{D3} = 0$. S is turned off, and D_2 and D_5 are turned on. D_1, D_3, and D_4 are turned off. Fig. 4(h)

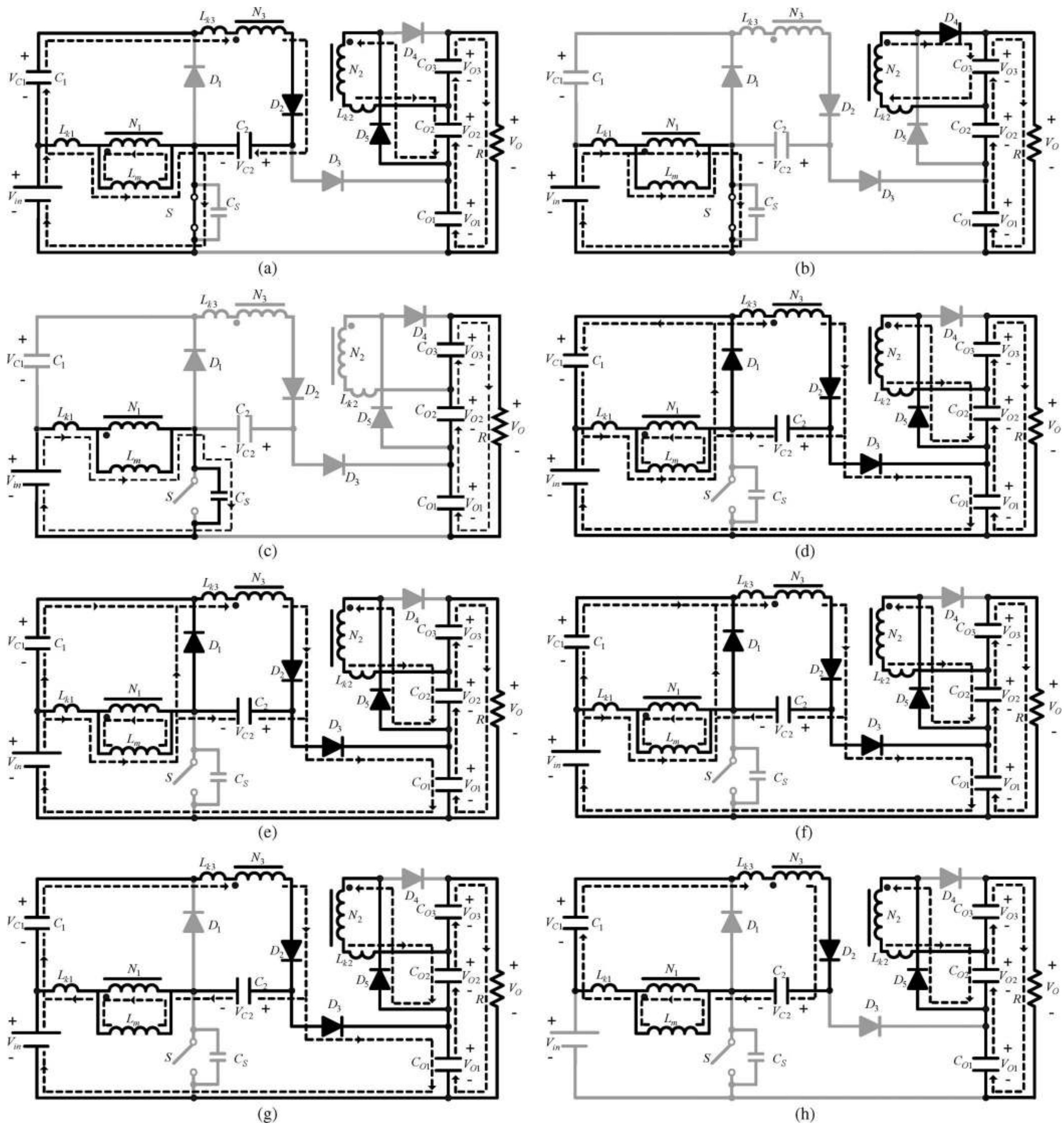

Fig. 4. Current-flow path of the operating modes for CCM operation. (a) Mode 1. (b) Mode 2. (c) Mode 3. (d) Mode 4. (e) Mode 5. (f) Mode 6. (g) Mode 7. (h) Mode 8.

illustrates the current-flow path of the proposed converter in this mode. The energy stored in L_m is still released to C_2 and C_{O2} via N_2 and N_3 in this mode. This mode is ended at $t = t_8$ when switch S is turned on.

In order to analyze the CCM steady-state characteristics simply, the leakage inductors of the N_2 and N_3 windings, L_{k2} and L_{k3}, are neglected. Moreover, the durations of modes 1 and 3 are neglected since the time of these modes is very short.

During the switch-on period, V_{Lm} and V_{O3} can be written as

$$V_{Lm} = kV_{\text{in}} \tag{4}$$

$$V_{O3} = n_2 k V_{\text{in}} \tag{5}$$

where k is the coupling coefficient of the coupled inductor, $k = L_m/(L_m + L_{k1})$.

During the switch-off period, the energy stored in L_{k1} is released to clamp capacitor C_1. Due to the steady-state condition of C_1 [27], [32], the energy release cycle of the primary leakage inductor D_{C1} can be denoted as

$$D_{C1} = \frac{t_{C1}}{T} = \frac{2(1-D)}{n_2+1} \tag{6}$$

where T is the switching period, D is the duty ratio of the switch, and t_{C1} is the time duration of mode 4.

By applying the voltage-second balance on L_m and L_{k1}, V_{Lm} and V_{Lk1} are derived as

$$V_{Lm} = \frac{kD}{1-D} V_{\text{in}} \tag{7}$$

$$V_{Lk1} = \frac{D(n_2+1)(1-k)}{2(1-D)} V_{\text{in}}. \tag{8}$$

Thus, the voltages across C_1 and C_2 can be written by (7) and (8) as

$$V_{C1} = V_{Lk1} + V_{Lm} = \left[\frac{D(n_2+1)(1-k)}{2(1-D)} + \frac{kD}{1-D}\right] V_{\text{in}} \tag{9}$$

$$V_{C2} = n_3 V_{Lm} = \frac{n_3 kD}{1-D} V_{\text{in}}. \tag{10}$$

According to (7), (9), and (10), the voltages across C_{O1} and C_{O2} can be presented as

$$V_{O1} = V_{C2} + V_{C1} + V_{\text{in}} = \left[\frac{kD(n_3+1)+1-D}{1-D} + \frac{D(n_2+1)(1-k)}{2(1-D)}\right] V_{\text{in}} \tag{11}$$

$$V_{O2} = n_2 V_{Lm} = \frac{n_2 kD}{1-D} V_{\text{in}}. \tag{12}$$

From (5), (11), and (12), the output voltage V_O is expressed as

$$V_O = V_{O1} + V_{O2} + V_{O3} = \left[n_2 k + \frac{kD(n_3+1)+1-D+n_2 kD}{1-D} + \frac{D(n_2+1)(1-k)}{2(1-D)}\right] V_{\text{in}}. \tag{13}$$

Fig. 5 shows the voltage gain versus the duty ratio under various coupling coefficients of the coupled inductor and the same turn ratios $n_2 = n_3$. It illustrates that the coupling coefficient results the voltage gain decline. However, the decline in the voltage gain is less sensitive to the coupling coefficient k. Therefore, the ideal voltage gain and the voltage across C_1 and C_2 can be rewritten as

$$V_O = V_{O1} + V_{O2} + V_{O3} = \left[n_2 + \frac{1+(n_2+n_3)D}{1-D}\right] V_{\text{in}} \tag{14}$$

$$V_{C1} = \frac{D}{1-D} V_{\text{in}} \tag{15}$$

$$V_{C2} = \frac{n_3 D}{1-D} V_{\text{in}} \tag{16}$$

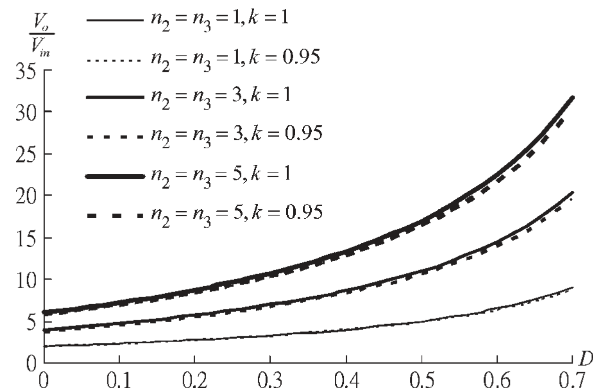

Fig. 5. Voltage gain versus duty ratio under various turn ratios and coupling coefficients of the coupled inductor.

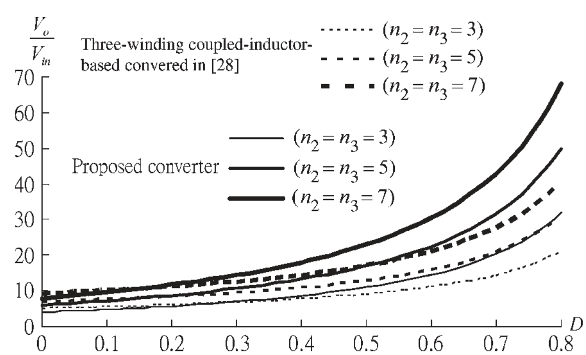

Fig. 6. Voltage gain versus duty ratio of the proposed converter and the counterpart.

when $k = 1$. This figure can also be used to determine the maximum operating duty ratio and the turn ratios of the coupled inductor.

Equation (14) indicates that the proposed converter achieves a high voltage gain by utilizing the techniques of the voltage doubler and the coupled inductor.

Fig. 6 shows the voltage gain against the duty ratio when $n_2 = n_3$ of both the proposed converter and the three-winding coupled-inductor-based converter in [28]. Based on Fig. 6, the voltage gain of the proposed converter exceeds that of the counterpart in [28], when the converters operate at a larger duty ratio particularly. The result reveals that the proposed converter has a high-voltage-gain performance indeed. Moreover, since the coupled inductor operated as forward and flyback converters, the utilization rate of the magnetic core of the coupled inductor can be improved.

According to the aforementioned analysis, the voltage stresses on the switch and the diodes are as follows:

$$V_{DS} = V_{D1} = V_{D3} = \frac{1}{1-D} V_{\text{in}} \tag{17}$$

$$V_{D2} = \frac{n_3 - 1}{1-D} V_{\text{in}} \tag{18}$$

$$V_{D4} = V_{D5} = \frac{n_2}{1-D} V_{\text{in}}. \tag{19}$$

Equations (14) and (17) reveal that the voltage stress on the main switch is clamped at a low voltage, and which is lower than the output voltage. Equations (17)–(19) can be adopted to determine the maximum voltage stress on each power device.

B. DCM

To simplify the discontinuous conduction mode (DCM) analysis, all leakage inductors of the coupled inductor are neglected. The coupled inductor is modeled as a magnetizing inductor L_m. All semiconductor components are assumed as ideal. The operating modes of the DCM operation can be divided into three modes during each switching period. Fig. 7 shows the equivalent circuit of the proposed converter and the key waveforms under DCM operation in one switching period. i_L, V_{N2}, and V_{N3} are denoted as that in Fig. 7(a). The operating modes are described as follows.

Mode 1 (t_0–t_1): At $t = t_0$, S is turned on, D_1, D_2, D_3, and D_5 are turned off, and D_4 is turned on. The current-flow path of the proposed converter in this mode is shown in Fig. 8(a). In this interval, the inductor L_m is charged from the dc input voltage V_{in}. The current i_{Lm} is increased linearly. The voltage across C_{O3} is charged to n_2V_{in}. The load energy is supplied by the capacitors C_{O1}, C_{O2}, and C_{O3}. This mode is ended at $t = t_1$ when switch S is turned off. Thus, the equations are written as

$$V_{Lm} = V_{\text{in}} \tag{20}$$

$$I_{Lmp} = \frac{V_{\text{in}}}{L_m}DT \tag{21}$$

$$V_{N2} = n_2V_{\text{in}} \tag{22}$$

$$V_{N3} = n_3V_{\text{in}} \tag{23}$$

where I_{Lmp} denotes the peak value of the magnetizing current.

Mode 2 (t_1–t_2): At $t = t_1$, S is turned off, D_1, D_2, D_3, and D_5 are turned on, and D_4 is turned off. Fig. 8(b) shows the current-flow path of the proposed converter in this mode. In this interval, the energy stored in L_m is released to C_1, C_2, C_{O1}, and C_{O2}; thus, i_{D1}, i_{D2}, i_{D3}, and i_{D5} are decreased linearly. The equations are given as

$$V_{Lm} = -V_{C1} = V_{C2} + V_{\text{in}} - V_{O1} \tag{24}$$

$$I_{Lmp} = \frac{V_{C1}}{L_m}D_LT \tag{25}$$

$$I_{D3p} = \frac{I_{Lmp}}{2 + n_2 + n_3} \tag{26}$$

$$V_{N2} = -n_2V_{C1} = -V_{O2} \tag{27}$$

$$V_{N3} = -V_{C2} = V_{\text{in}} + V_{C1} - V_{O1} \tag{28}$$

where I_{D3p} denotes the peak value of i_{D3}. This mode ends at $t = t_2$ when the magnetizing current i_{Lm} reaches zero.

Mode 3 (t_2–t_3): At $t = t_2$, i_{Lm} is equal to zero. S is still turned off, and D_1, D_2, D_3, D_4, and D_5 are also turned off. Fig. 8(c) illustrates the current-flow path of the proposed converter in this mode. The energies stored in C_{O1}, C_{O2}, and C_{O3} are released to the load during this interval. This mode is ended at $t = t_3$ when switch S is turned on.

By using the voltage-second balance principle on L_m, N_2, and N_3 of the coupled inductor, the following equations are given as

$$\int_0^{DT} V_{\text{in}}\,dt + \int_{DT}^{(D+D_L)T} (-V_{C1})\,dt = 0 \tag{29}$$

$$\int_0^{DT} n_2V_{\text{in}}\,dt + \int_{DT}^{(D+D_L)T} (-V_{O2})\,dt = 0 \tag{30}$$

$$\begin{aligned}\int_0^{DT} n_3V_{\text{in}}\,dt &+ \int_{DT}^{(D+D_L)T} (V_{\text{in}} + V_{C1} - V_{O1})\,dt \\ &= \int_0^{DT} n_3V_{\text{in}}\,dt + \int_{DT}^{(D+D_L)T} (-V_{C2})\,dt = 0.\end{aligned} \tag{31}$$

From (29)–(31), V_{C1}, V_{C2}, V_{O1}, and V_{O2} are derived as

$$V_{C1} = \frac{D}{D_L}V_{\text{in}} \tag{32}$$

$$V_{C2} = n_3\frac{D}{D_L}V_{\text{in}} \tag{33}$$

$$V_{O2} = n_2\frac{D}{D_L}V_{\text{in}} \tag{34}$$

$$V_{O1} = \left[(n_3+1)\frac{D}{D_L} + 1\right]V_{\text{in}}. \tag{35}$$

Since V_{O3} is kept to n_2V_{in} during one switching period, thus, from (34) and (35), the output voltage V_O is expressed as

$$\begin{aligned}V_O &= V_{O1} + V_{O2} + V_{O3} \\ &= \left[n_2 + (1 + n_2 + n_3)\frac{D}{D_L} + 1\right]V_{\text{in}}.\end{aligned} \tag{36}$$

According to (36), D_L can be derived as

$$D_L = \frac{(1 + n_2 + n_3)DV_{\text{in}}}{V_O - (1 + n_2)V_{\text{in}}}. \tag{37}$$

From Fig. 7(b), the average value of i_{CO1} is computed as

$$\begin{aligned}I_{CO1} &= \frac{\frac{1}{2}D_LT\frac{I_{Lmp}}{n_2+n_3+2} - I_OT}{T} \\ &= \frac{1}{2}D_L\frac{I_{Lmp}}{2 + n_2 + n_3} - I_O.\end{aligned} \tag{38}$$

Under steady state, I_{CO1} is equal to zero. Thus, substituting (25), (37), and $I_{CO1} = 0$ into (38), the following equation is obtained as

$$\frac{(1 + n_2 + n_3)D^2V_{\text{in}}^2T}{2\left[V_O - (1 + n_2)V_{\text{in}}\right](2 + n_2 + n_3)L_m} = \frac{V_O}{R}. \tag{39}$$

The normalized inductor time constant is then defined as

$$\tau_L = \frac{L_mf}{R} \tag{40}$$

where f is the switching frequency.

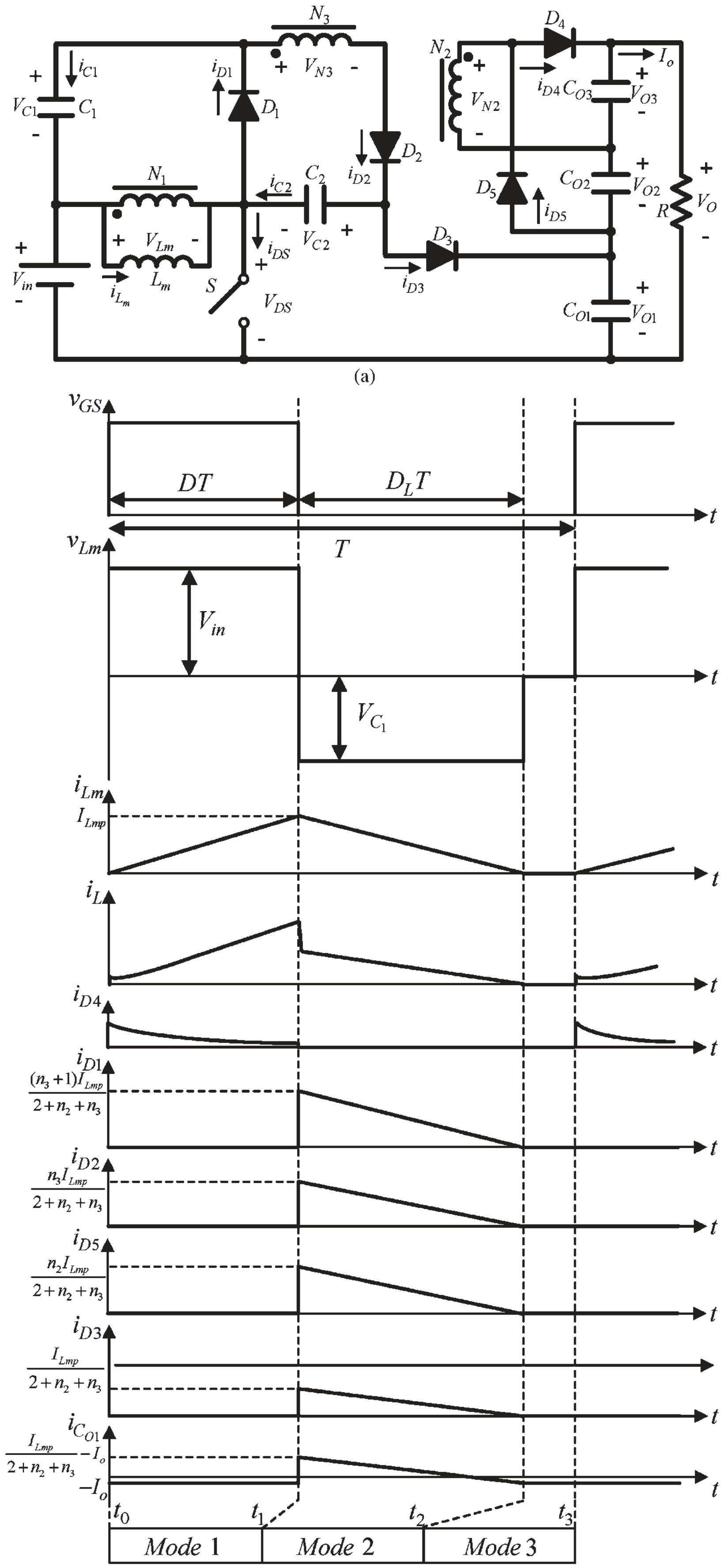

Fig. 7. (a) Equivalent circuit of the proposed converter of the DCM. (b) Some typical waveforms under DCM operation in one switching period.

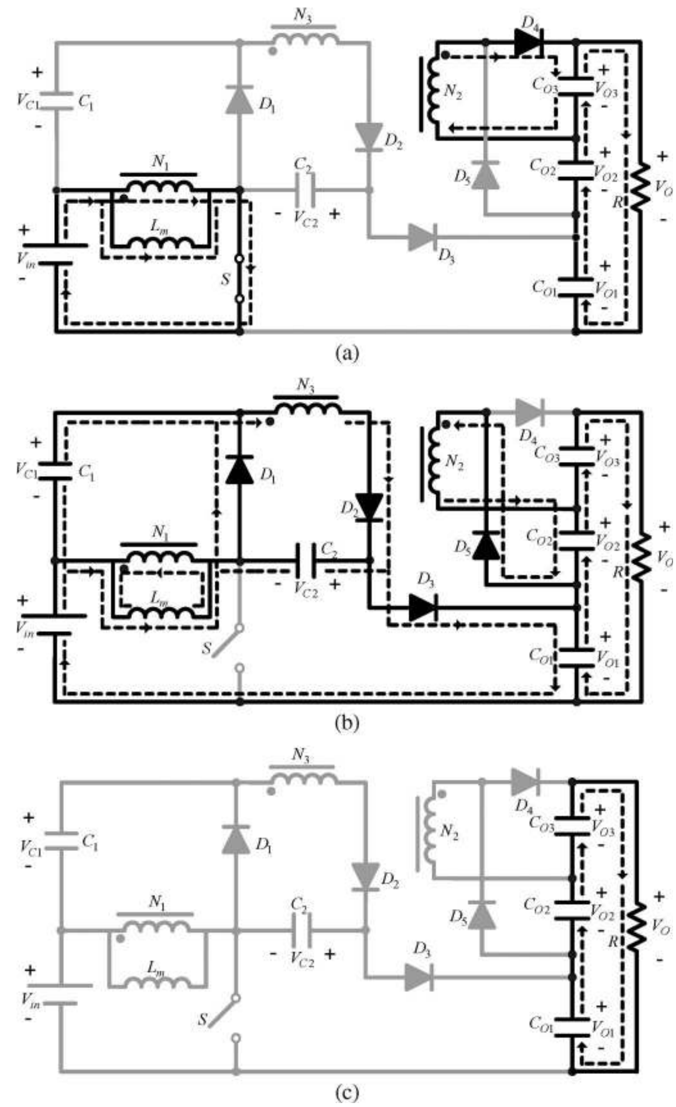

Fig. 8. Current-flow path of the operating modes for DCM operation. (a) Mode 1. (b) Mode 2. (c) Mode 3.

Substituting (40) into (39), the DCM voltage gain is expressed as

$$\frac{V_O}{V_{\text{in}}} = \frac{1+n_2}{2} + \sqrt{\frac{(1+n_2)^2}{4} + \frac{(1+n_2+n_3)D^2}{2\tau_L(2+n_2+n_3)}}. \quad (41)$$

If the proposed converter is operated in the boundary conduction mode (BCM), then the voltage gain of the CCM operation is equal to the voltage gain of the DCM operation. From (14) and (41), the boundary normalized inductor time constant τ_{LB} can be derived as

$$\tau_{LB} = \frac{D(1-D)^2}{2(2+n_2+n_3)(1+n_2+n_3 D)}. \quad (42)$$

Fig. 9 plots the curves of the boundary normalized inductor time constant τ_{LB} versus the duty ratio under $n_2 = n_3 = 2.7$. The proposed converter is operated in CCM if $\tau_L > \tau_{LB}$, and otherwise in DCM.

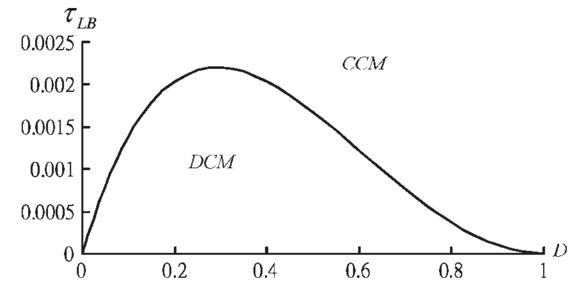

Fig. 9. Boundary normalized inductor time constant versus duty ratio (assuming $n_2 = n_3 = 2.7$).

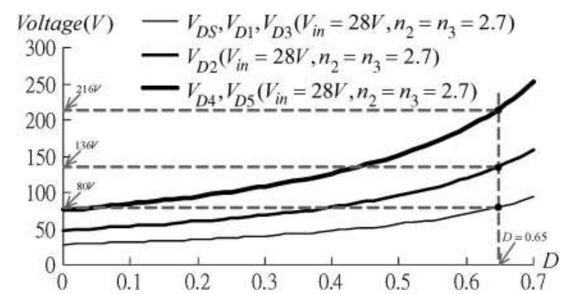

Fig. 10. Voltage stresses of each power device versus duty ratio under fixed coupled-inductor turn ratios, $n_2 = n_3 = 2.7$.

III. Design and Experiment of the Proposed Converter

In order to verify the performances of the designed proposed converter for a fuel cell energy conversion system, a PEMFC system is adopted for the input power source of the proposed converter. The PEMFC system used in this paper is the Ballard Nexa 1.2-kW power stack module, which is manufactured by Ballard Power Systems Company. The specifications of the laboratory prototype converter are as follows:

1) input dc voltage V_{in}: 28–40 V;
2) output dc voltage V_O: 400 V;
3) maximum output power: 750 W;
4) switching frequency: 50 kHz.

The on resistance of the power switch and the primary winding of the coupled inductor result much conduction loss for the low input power source of the proposed converter. Therefore, the maximum operating duty ratio is selected as a reasonable duty ratio for the high-current issue in this design. The maximum duty ratio is selected nearly 0.65. In addition, the turn ratios n_2 and n_3 are assumed to be equal. Thus, referring to Fig. 5, the turn ratios n_2 and n_3 and the maximum duty ratio are selected as 2.7 and 0.65, respectively.

From (17)–(19), Fig. 10 plots the voltage stress of each power device under various duty ratios when $n_2 = n_3 = 2.7$. This figure can be used to find the maximum voltage rating for each power device.

Based on the aforementioned circuit design and analysis, the following key components are selected:

1) power switch S: NTY100N10, n-channel MOSFET;
2) diodes D_1 and D_3: MUR20H150, Schottky diode;

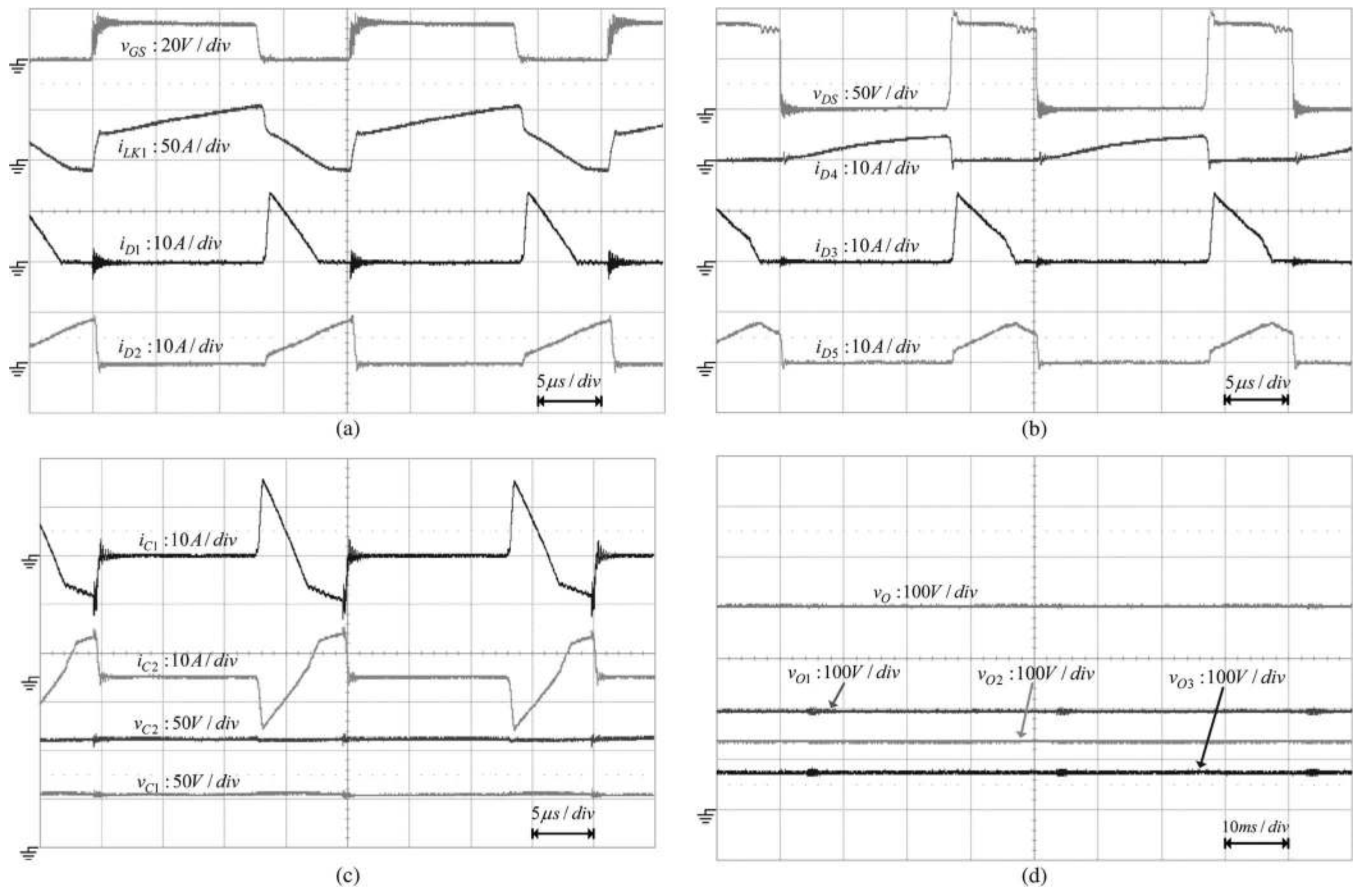

Fig. 11. Experimental results of the proposed converter under full-load $P_O = 750$ W and $V_{\text{in}} = 28.9$ V.

3) diode D_2: MUR20200CT, Schottky diode;
4) diodes D_4 and D_5: DSEK 60, ultrafast diode;
5) coupled inductor: ETD-59 core; PC-40; N_1, N_2, and $N_3 =$ 1, 2.7, and 2.7, respectively; $L_m = 20$ μH; $L_{k1} = 0.25$ μH;
6) capacitor C_1: 23.5-μF/100-V metallized polyester film capacitor;
7) capacitor C_2: 19.8-μF/250-V metallized polyester film capacitor;
8) capacitors C_{O1}, C_{O2}, and C_{O3}: 220-μF/250-V aluminum capacitor.

Fig. 11 shows the measured waveforms for full-load $P_O =$ 750 W and $V_{\text{in}} = 28.9$ V. The proposed converter is operated at CCM under full-load condition. The measured waveforms agree with the steady-state analysis and circuit design. From Fig. 11(b), V_{DS} is clamped at approximately 90 V during the switch-off period. The voltage stress of the switch is effectively clamped without any snubber circuit. Therefore, a low-voltage-rating power switch with a low on resistance for the high-efficiency conversion of the proposed converter is adopted. Fig. 11(c) shows the dc voltage levels across C_1 and C_2, which reveals that V_{C1} and V_{C2} satisfy (15) and (16). Also, Fig. 11(d) indicates that V_O is the summation of V_{O1}, V_{O2}, and V_{O3}, which is consistent with (14).

Fig. 12 shows the measured waveforms at light-load $P_O =$ 115 W and $V_{\text{in}} = 36.7$ V. The proposed converter is operated in DCM under light load. From Fig. 12(b), V_{DS} is still effectively clamped at around 90 V.

Fig. 13 demonstrates the proposed converter under boundary condition at $D = 0.56$, $P_O = 250$ W, and $V_{\text{in}} = 33.5$ V, approximately. This figure is consistent with (42).

Fig. 14 shows the experimental conversion efficiency of the proposed converter and the fuel cell voltage under various output powers. From the results, the output voltage of the fuel cell depends on the output power variations, which almost decreases linearly as the output power increases linearly. The maximum efficiency was around 96.7% at $P_O = 115$ W and $V_{\text{in}} = 36.7$ V. The full-load efficiency was approximately 91% at $V_{\text{in}} = 28.9$ V. The results verify that the proposed converter has high-efficiency conversion, which is higher than conventional converters. Since the low input voltage is applied in this energy conversion system, the input of the proposed converter should suffer very high current, which results much conduction loss during the switch-on period. Thus, it will result in lower conversion efficiency. Furthermore, the proposed converter uses only one active switch for the energy conversion, which also suffers very high current during the switch-on period. Thus, the proposed converter is suitable for low-to-middle-power applications. In order to reduce the switch conduction loss, the switches in parallel are usually adopted for this high-current issue to improve efficiency. This approach can also be used for the proposed converter in high-power applications. Moreover, the high step-up converter [29], [30] uses two active switches to share the input current by interleaved operation; therefore, the low input conduction loss for high efficiency is presented.

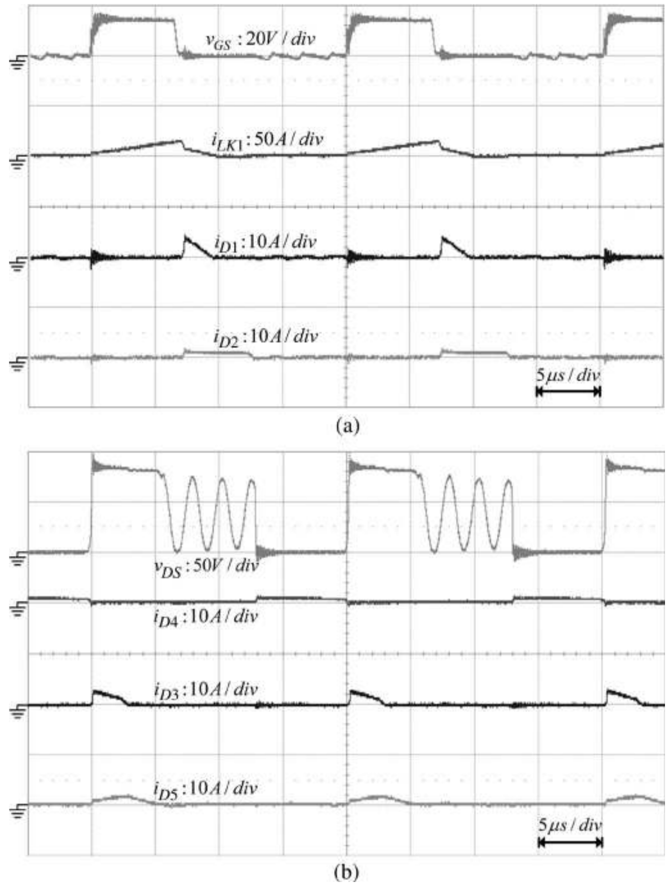

Fig. 12. Experimental results of the proposed converter under light-load $P_O = 115$ W and $V_{\mathrm{in}} = 36.7$ V.

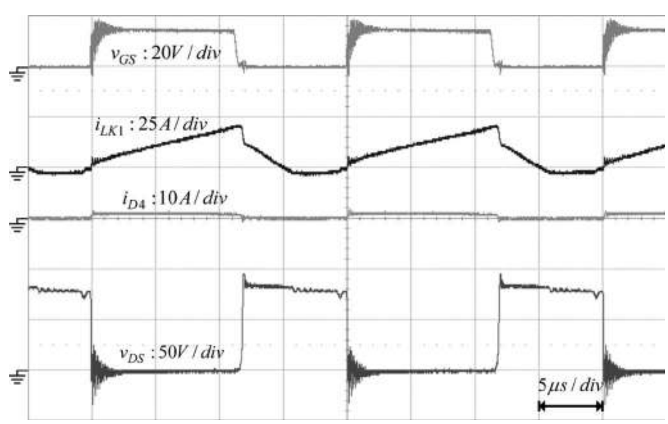

Fig. 13. Experimental results of the proposed converter under BCM condition $D = 0.56$, $P_O = 250$ W, and $V_{\mathrm{in}} = 33.5$ V.

These converters are suitably used for high-power applications due to the low-level current on the active switches.

IV. Conclusion

A novel high step-up dc–dc converter, which utilizes a voltage doubler and adjusts the turn ratios of the coupled inductor, has been proposed to achieve high step-up voltage gain in this paper. The proposed converter has been highly efficient because it recycles the energy stored in the leakage inductor of the coupled inductor. Since the voltage across the active switch is

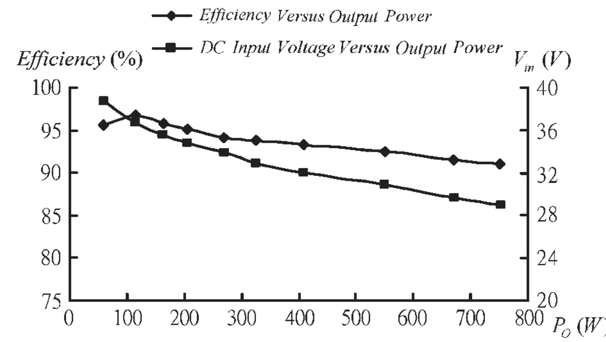

Fig. 14. Experimental conversion efficiency and fuel cell voltage for PEMFC under various output powers.

clamped, the low-voltage-rating and low-on-resistance power switch can be selected to improve efficiency. The operating principles and the steady-state analysis have been described in detail. Also, the boundary condition has been obtained. Finally, a prototype converter has been implemented to verify the performance of the proposed converter, which is supplied by a PEMFC. The measured waveforms have been consistent with the steady-state analysis, and the voltage stress on the switch has been effectively clamped. The experimental results have indicated that the full-load efficiency was 91% at $V_{\mathrm{in}} = 28.9$ V. The maximum efficiency was 96.7% at $P_O = 115$ W and $V_{\mathrm{in}} = 36.7$ V. Thus, the proposed converter is suitable for power conversion systems, such as fuel-cell- and solar-cell-based power conversion systems, high-intensity discharge lamps for automobile headlamps, and others.

References

[1] J. M. Correa, F. A. Farret, N. Canha, and M. G. Simoes, "An electrochemical-based fuel-cell model suitable for electrical engineering automation approach," *IEEE Trans. Ind. Electron.*, vol. 51, no. 5, pp. 1103–1112, Oct. 2004.

[2] Z. Jiang and R. A. Dougal, "A compact digitally controlled fuel cell/battery hybrid power source," *IEEE Trans. Ind. Electron.*, vol. 53, no. 4, pp. 1094–1104, Aug. 2006.

[3] S. M. Lukic, J. Cao, R. C. Bansal, F. Rodriguez, and A. Emadi, "Energy storage systems for automotive applications," *IEEE Trans. Ind. Electron.*, vol. 55, no. 6, pp. 2258–2267, Jun. 2008.

[4] H. Tao, J. L. Duarte, and M. A. M. Hendrix, "Line-interactive UPS using a fuel cell as the primary source," *IEEE Trans. Ind. Electron.*, vol. 55, no. 8, pp. 3012–3021, Aug. 2008.

[5] M. W. Ellis, M. R. V. Spakovsky, and D. J. Nelson, "Fuel cell systems: Efficient, flexible energy conversion for the 21st century," *Proc. IEEE*, vol. 89, no. 12, pp. 1808–1818, Dec. 2001.

[6] C. Wang, M. H. Nenrir, and S. R. Shaw, "Dynamic models and model validation for PEM fuel cells using electrical circuits," *IEEE Trans. Energy Convers.*, vol. 20, no. 2, pp. 442–451, Jun. 2005.

[7] R. W. Erickson and D. Maksimovic, *Fundamentals of Power Electronics*. Norwell, MA: Kluwer, 2001, pp. 39–55.

[8] N. Mohan, T. M. Undeland, and W. P. Robbins, *Power Electronic: Converters, Applications and Design*. New York: Wiley, 1995, pp. 172–178.

[9] J. Wang, F. Z. Peng, J. Anderson, A. Joseph, and R. Buffenbarger, "Low cost fuel cell converter system for residential power generation," *IEEE Trans. Power Electron.*, vol. 19, no. 5, pp. 1315–1322, Sep. 2004.

[10] R. Sharma and H. Cao, "Low cost high efficiency DC–DC converter for fuel cell powered auxiliary power unit of a heavy vehicle," *IEEE Trans. Power Electron.*, vol. 21, no. 3, pp. 587–597, May 2006.

[11] S. J. Finney, B. W. Williams, and T. C. Green, "RCD snubber revisited," *IEEE Trans. Ind. Appl.*, vol. 32, no. 1, pp. 155–160, Jan./Feb. 1996.

[12] D. D. C. Lu, D. K. W. Cheng, and Y. S. Lee, "A single-switch continuous conduction-mode boost converter with reduced reverse-recovery and switching losses," *IEEE Trans. Ind. Electron.*, vol. 50, no. 4, pp. 767–776, Aug. 2003.

[13] Y. S. Lee and B. T. Lin, "Adding active clamping and soft switching to boost–flyback single-stage isolated power-factor-corrected power supplies," *IEEE Trans. Power Electron.*, vol. 12, no. 6, pp. 1017–1027, Nov. 1997.

[14] C. M. C. Duarte and I. Barbi, "An improved family of ZVS-PWM active-clamping DC-to-DC converters," *IEEE Trans. Power Electron.*, vol. 17, no. 1, pp. 1–7, Jan. 2002.

[15] T. F. Wu, Y. S. Lai, J. C. Hung, and Y. M. Chen, "Boost converter with coupled inductors and buck–boost type active clamp," *IEEE Trans. Ind. Electron.*, vol. 55, no. 1, pp. 154–162, Jan. 2008.

[16] W. Cheng, X. C. Liu, and Y. S. Lee, "A new improved boost converter with ripple free input current using coupled inductors," in *Proc. IEE Int. Conf. Power Electron. Variable Speed Drives*, London, U.K., 1998, pp. 592–599.

[17] J. Wang, W. G. Dunford, and K. Monrad, "Analysis of a ripple-free input-current boost converter with discontinuous conduction characteristics," *IEEE Trans. Power Electron.*, vol. 12, no. 4, pp. 684–694, Jul. 1997.

[18] K. C. Tseng and T. J. Liang, "Novel high-efficiency step-up converter," *Proc. Inst. Elect. Eng.—Elect. Power Appl.*, vol. 151, no. 2, pp. 182–190, Mar. 2004.

[19] T. J. Liang and K. C. Tseng, "Analysis of integrated boost–flyback step-up converter," *Proc. Inst. Elect. Eng.—Elect. Power Appl.*, vol. 152, no. 2, pp. 217–225, Mar. 2005.

[20] T. Dumrongkittigule, V. Tarateeraseth, and W. Khan-ngern, "A new integrated inductor balanced switching technique for common mode EMI reduction in high step-up DC/DC converter," in *Proc. 17th Int. Zurich Symp. Electromagn. Compat.*, Singapore, 2006, pp. 541–544.

[21] K. B. Park, H. W. Seong, H. S. Kim, G. W. Moon, and M. J. Youn, "Integrated boost–sepic converter for high step-up applications," in *Proc. IEEE Power Electron. Spec. Conf.*, Rhodes, Greece, 2008, pp. 944–950.

[22] J. W. Baek, M. H. Ryoo, T. J. Kin, D. W. Yoo, and J. S. Kim, "High boost converter using voltage multiplier," in *Proc. IEEE IECON*, Raleigh, NC, 2005, pp. 1–6.

[23] J. Y. Lee and S. N. Hwang, "Non-isolated high-gain boost converter using voltage-stacking cell," *Electron. Lett.*, vol. 44, no. 10, pp. 644–645, May 2008.

[24] F. L. Luo and H. Ye, "Positive output super-lift converters," *IEEE Trans. Power Electron.*, vol. 18, no. 1, pp. 105–113, Jan. 2003.

[25] F. L. Luo and H. Ye, "Positive output multiple-lift push–pull switched-capacitor Luo-converters," *IEEE Trans. Ind. Electron.*, vol. 51, no. 3, pp. 594–602, Jun. 2004.

[26] R. J. Wai and R. Y. Duan, "High-efficiency DC/DC converter with high voltage gain," *Proc. Inst. Elect. Eng.—Elect. Power Appl.*, vol. 152, no. 4, pp. 793–802, Jul. 2005.

[27] R. J. Wai and R. Y. Duan, "High converter with coupled-inductor," *IEEE Trans. Power Electron.*, vol. 20, no. 5, pp. 1025–1035, Sep. 2005.

[28] R. J. Wai, C. Y. Lin, R. Y. Duan, and Y. R. Chang, "High-efficiency DC–DC converter with high voltage gain and reduced switch stress," *IEEE Trans. Ind. Electron.*, vol. 54, no. 1, pp. 354–364, Feb. 2007.

[29] S. V. Araujo, R. P. T. Bascope, G. V. T. Bascope, and L. Menezes, "Step-up converter with high voltage gain employing three-state switching cell and voltage multiplier," in *Proc. IEEE Power Electron. Spec. Conf.*, Rhodes, Greece, 2008, pp. 2271–2277.

[30] Y. J. A. Alcazar, R. T. Bascope, D. S. de Oliveira, E. H. P. Andrade, and W. G. Cardenas, "High voltage gain boost converter based on three-state switching cell and voltage multipliers," in *Proc. IEEE IECON Conf.*, Orlando, FL, 2008, pp. 2346–2352.

[31] O. Krykunov, "Analysis of the extended forward converter for fuel cell applications," in *Proc. ISIE Conf.*, Cambridge, U.K., 2008, pp. 661–666.

[32] Q. Zhao and F. C. Lee, "High-efficiency, high step-up DC–DC converters," *IEEE Trans. Power Electron.*, vol. 18, no. 1, pp. 65–73, Jan. 2003.

Shih-Kuen Changchien was born in Kaohsiung, Taiwan, in 1967. He received the M.S. degree in electrical engineering from Da-Yeh University, Changhua City, Taiwan, in 1997, and the Ph.D. degree in electrical engineering from National Cheng Kung University (NCKU), Tainan, Taiwan, in 2009.

Since August 2001, he has been with the Department of Electrical Engineering, Chienkuo Technology University, Changhua City, where he is currently an Assistant Professor. His research interests include power converters, power factor correction, and renewable energy conversion.

Tsorng-Juu Liang (M'93) was born in Kaohsiung, Taiwan. He received the B.S. degree in electrophysics from National Chiao Tung University, Hsinchu, Taiwan, in 1985, and the M.S. and Ph.D. degrees in electrical engineering from the University of Missouri, Columbia, in 1990 and 1993, respectively.

From June 1987 to May 1989, he was a Research and Design Engineer with TECO Electric and Machinery Company, Taiwan. From 1990 to 1993, he was a Research Assistant with the Power Electronics Research Center, University of Missouri. From 1993 to 1998, he was an Assistant Professor in the Department of Electrical Engineering, Kaohsiung Polytechnic Institute, Kaohsiung. Since 1998, he has been with the Department of Electrical Engineering, National Cheng Kung University, Tainan, Taiwan, where he was the Director with the Electrical Laboratories from 2001 to 2004 and is currently a Professor. His research interests are inverter design, electronic ballast, dc-to-dc converters, switching power supplies, back light inverters, renewable energy conversion, power integrated circuits, and high-power applications.

Dr. Liang is a member of the IEEE Power Electronics, IEEE Industrial Electronics, IEEE Circuits and Systems, and IEEE Industry Applications Societies.

Jiann-Fuh Chen (S'79–M'80) was born in Chung-Hua, Taiwan, in 1955. He received the B.S., M.S., and Ph.D. degrees in electrical engineering from National Cheng Kung University (NCKU), Tainan, Taiwan, in 1978, 1980, and 1985, respectively.

Since 1980, he has been with the Department of Electrical Engineering, NCKU, where he is currently a Professor and the Director. His research interests are power electronics and energy conversion.

Lung-Sheng Yang was born in Tainan, Taiwan, in 1967. He received the B.S. degree in electrical engineering from National Taiwan Institute of Technology, Taipei, Taiwan, in 1990, the M.S. degree in electrical engineering from National Tsing Hua University, Hsinchu, Taiwan, in 1992, and the Ph.D. degree in electrical engineering from National Cheng Kung University (NCKU), Tainan, in 2007.

He is currently a Postdoctoral Researcher in the Department of Electrical Engineering, NCKU. His research interests are power factor correction, dc–dc converters, renewable energy conversion, and electronic ballast.